Journal of
Materials Chemistry

Cite this: J. Mater. Chem., 2012, **22**, 909

www.rsc.org/materials

PAPER

Zinc-1,4-benzenedicarboxylate-bipyridine frameworks – linker functionalization impacts network topology during solvothermal synthesis†

Sebastian Henke,[a] Andreas Schneemann,[a] Shobhna Kapoor,[b] Roland Winter[b] and Roland A. Fischer*[a]

Received 26th September 2011, Accepted 18th October 2011
DOI: 10.1039/c1jm14791a

Substitution of 1,4-benzenedicarboxylate (bdc) with additional alkoxy chains is the key to construct a family of metal–organic frameworks (MOFs) of the type $[Zn_2(\text{fu-bdc})_2(\text{bipy})]_n$ (fu-bdc = functionalized bdc; bipy = 4,4′-bipyridine) exhibiting a honeycomb-like topology instead of the default pillared square-grid topology. Both the substitution pattern of the phenyl ring of the fu-bdc linker and the chain length of the alkoxy substituents have a major impact on the structure of the derived frameworks. Substitution at positions 2 and 3 leads to the trivial pillared square-grid framework, and substitution at positions 2 and 5 or 2 and 6 yields MOFs with the honeycomb-like topology. Also, simple methoxy substituents lead to the construction of a pillared square-grid topology, whereas longer substituents like ethoxy, *n*-propoxy, and *n*-butoxy generate honeycomb-like framework structures. These honeycomb MOFs feature one-dimensional channels, which are tuneable in diameter and functionality by the choice of substituent attached to the bdc-type linker. Pure component sorption isotherms indicate that the honeycomb-like frameworks selectively adsorb CO_2 over N_2 and CH_4.

Introduction

The rapidly growing family of metal–organic frameworks (MOFs) or porous coordination polymers (PCPs) represents highly porous hybrid materials constructed from inorganic building units and organic linkers.[1] A modular building principle allows the isoreticular synthesis of network topologies with large specific surface areas and high pore volumes. In contrast to strictly inorganic porous materials, like zeolites, additional functional groups or substituents can be implemented in the pores *via* extensive modification of the organic building blocks.[2] This allows a targeted tailoring of specific properties, focussing on a great variety of possible applications, for example in gas storage,[3] gas separation,[4] catalysis,[5] optics,[6] or chemical sensing.[7]

Due to the great diversity in the accessible inorganic and organic building units an enormous number of different MOFs has been prepared so far.[1,2] It has been shown that the diversity of MOF structures can not only be controlled by the choice of inorganic and organic building bricks, but also by the utilized solvent, the reaction temperature, or molecular templates.[8] However, an important field is the targeted construction of novel MOF topologies, by covalent functionalization of the linker molecules, because this allows the intrinsic properties of the linker to be influenced.[9] A prerequisite is that the functionalization should not interfere with the formation of an open framework structure. Therefore, particular functionalization of a linker can modify the conformational flexibility, for example by affecting rotational barriers, which can be the key for the construction of formerly inaccessible network structures.

A well-studied family of MOFs are the pillared layer-based networks of composition $[M_2L_2P]_n$ with M = Zn, Cu, Ni, Co; L = linear dicarboxylate linker (*e.g.*, 1,4-benzenedicarboxylate, 1,4-naphthalenedicarboxylate); P = neutral pillar (*e.g.*, 1,4-diazabicyclo[2.2.2]octane, 4,4′-bipyridine).[10,11] All these structures are constructed from dinuclear metal paddlewheel units, which are linked by L to construct two-dimensional sheets of composition $[M_2L_2]_n$, which are most often of the square-grid type. However, Kagome type sheets can be synthesized for some Zn derivatives.[12] The pillar P coordinates to the axial positions of the paddlewheel building units to interconnect the two-dimensional sheets and to generate a three-dimensional network. Noteworthy, if longer pillars are used, for example 4,4′-bipyridine (bipy), 1,4-bis(4-pyridyl)benzene or *N*,*N*′-di(4-pyridyl)-1,4,5,8-naphthalenetetracarboxydiimide, the frameworks are commonly interpenetrated by a second independent network.[11]

Recently, we have communicated that specific functionalization of the linker 1,4-benzenedicarboxylate (bdc) can trigger the formation of an unexpected honeycomb-like network of analogous $[M_2L_2P]_n$ composition.[13] The framework $[Zn_2(2,5\text{-BME-bdc})_2(\text{bipy})]_n$ (**1**; with 2,5-BME-bdc = 2,5-bis(2-methoxyethoxy)-1,4-benzenedicarboxylate) crystallizes in the trigonal

---

[a] *Lehrstuhl für Anorganische Chemie II, Organometallics & Materials Chemistry, Ruhr-Universität Bochum, Universitätsstraße 150, 44780 Bochum, Germany. E-mail: roland.fischer@rub.de; Fax: +49 234-32-14174; Tel: +49 234-32-24174*
[b] *Lehrstuhl für Physikalische Chemie I, Technische Universität Dortmund, 442277 Dortmund, Germany*

† Electronic supplementary information (ESI) available: Single crystal X-ray diffraction data, PXRDs, TGAs, NMR and IR spectra. CCDC reference numbers 834509 and 834510. For ESI and crystallographic data in CIF or other electronic format see DOI: 10.1039/c1jm14791a

space group $R\bar{3}c$ and features one dimensional porous channels, which are populated by the flexible 2-methoxyethoxy substituents (Fig. 1). These flexible groups act as molecular gates for incoming guest molecules. Therefore, CO_2 is very selectively adsorbed in **1** compared to N_2 and CH_4. We have shown that the major prerequisite for the formation of this honeycomb-like framework structure instead of the default pillared layer-based structures is substitution of the bdc linker in positions 2 and 5.[13] Thus a rotation of the carboxylate groups from the plane of the phenyl ring is facilitated in 2,5-BME-bdc. In the solid-state structure of **1** one half of the 2,5-BME-bdc linkers have a conformation, whereby the carboxylate groups are twisted approx. 90° (Fig. 1, top). Obviously, that kind of conformation is very unfavourable for conventional bdc, and also for the mono-substituted linker ME-bdc (2-methoxyethoxy-1,4-benzenedicarboxylate). Consequently, $[Zn_2(bdc)_2(bipy)]_n$ and $[Zn_2(ME\text{-}bdc)_2(bipy)]_n$ crystallize in the default interpenetrated pillared square-grid framework.[10b–d,13]

An additional and important requirement for the construction of the novel honeycomb-like topology is that the metrics of the linker L and the co-ligand P must be similar. Note that analogous reactions of 2,5-BME-bdc with the shorter co-ligand 1,4-diazabicyclo[2.2.2]octane yield the expected pillared square-grid type network.[14]

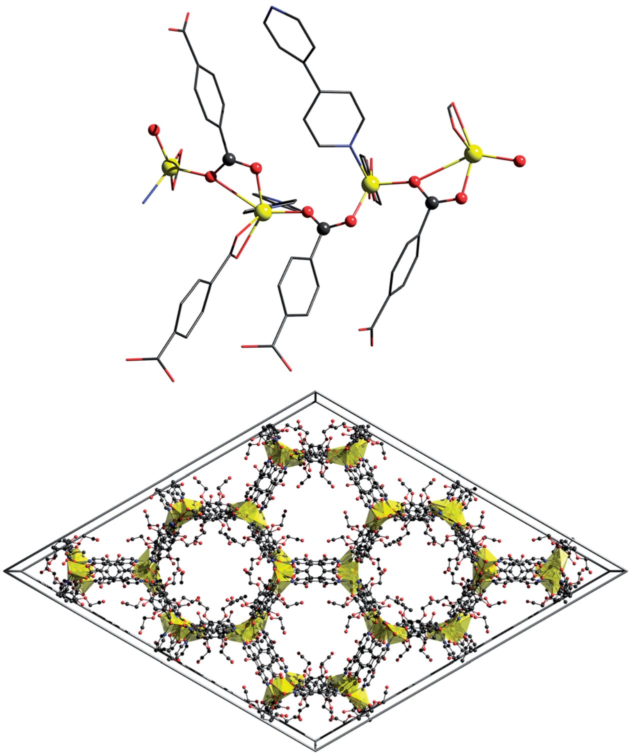

Fig. 1 Structure of as synthesized $[Zn_2(2,5\text{-BME-bdc})_2(bipy)]_n$ (**1as**).[13] Top: view of the infinite rod-like building unit consisting of Zn^{2+} centres, which are *syn–anti* bridged by carboxylates. The 2-methoxyethoxy groups have been omitted for clarity because they are highly disordered. Therefore, they could only be located partially in the structure. Bottom: view of the trigonal unit cell in the [001] direction ($a = b = 53.188(3)$ Å, $c = 17.813(2)$ Å; $\alpha = \beta = 90°$, $\gamma = 120°$; space group $R\bar{3}c$). Carbon, nitrogen, oxygen and zinc atoms are shown in dark grey, blue, red, and yellow, respectively. The polyhedra around the zinc centres are shown in yellow. Note that not all flexible 2-methoxyethoxy chains and no guest molecules could be localized in the electron density map due to severe disorder. Hydrogen atoms are omitted for the sake of clarity.

In this contribution we discuss the impact of the substitution pattern as well as the substituent chain length on the network topology of these $[Zn_2L_2(bipy)]_n$ coordination polymers more comprehensively. Therefore, the two substitution isomers of 2,5-BME-bdc, namely 2,3-bis(2-methoxyethoxy)-1,4-benzenedicarboxylate (2,3-BME-bdc) and 2,6-bis(2-methoxyethoxy)-1,4-benzenedicarboxylate (2,6-BME-bdc), were utilized as linker L in MOF synthesis together with zinc nitrate and bipy. In order to gain information about the impact of the substituent chain length we used four different alkoxy-functionalized bdc derivatives as linker L, in particular 2,5-dimethoxy-1,4-benzenedicarboxylate (DM-bdc), 2,5-diethoxy-1,4-benzenedicarboxylate (DE-bdc), 2,5-dipropoxy-1,4-benzenedicarboxylate (DP-bdc), and 2,5-dibutoxy-1,4-benzenedicarboxylate (DB-bdc). The derived MOFs of the general composition $[Zn_2L_2(bipy)]_n$ were characterised *via* single crystal X-ray diffraction and/or powder X-ray diffraction and spectroscopic techniques. Furthermore, the sorption properties of $[Zn_2(DE\text{-}bdc)_2(bipy)]_n$ and $[Zn_2(DB\text{-}bdc)_2(bipy)]_n$ were compared with the properties of the prototypic compound **1**.

Experimental section

General techniques, materials, and methods

All chemicals were purchased from commercial suppliers (Sigma-Aldrich, Fluka, Alfa Aesar, and others) and used without further purification. Elemental analyses were performed on a vario EL instrument from Elementar Hanau and AAS analyses were performed on an AAS 6 vario from Analytik Jena in the Microanalytical Laboratory of the Department of Analytical Chemistry at the Ruhr-Universität Bochum. Liquid phase NMR spectra were recorded on a Bruker Avance DPX-250 spectrometer (^1H, 250.1 MHz; ^{13}C, 62.9 MHz) at 293 K in $[D_6]$DMSO for the linkers and in $DCl/D_2O/[D_6]$DMSO for the digested MOF samples. ^{13}C NMR spectra were measured using an attached proton test (ATP) pulse program. Chemical shifts are given relative to TMS and were referenced to the solvent signals as internal standards. Solid-state ^{13}C MAS NMR spectra were recorded on a Bruker DSX-400 MHz spectrometer in ZrO_2 rotors of 2.5 mm diameter, applying pulse programs written by H.-J. Hauswald of the Department of Analytical Chemistry of the Ruhr-Universität Bochum. Infrared (IR) spectra were recorded on a Bruker Alpha-P FT-IR instrument in the ATR geometry equipped with a diamond ATR unit ($\tilde{\nu} = 4000\text{–}375\ cm^{-1}$) inside a glovebox (Ar atmosphere). Advanced IR measurements were performed at 25 °C with a Nicolet 5700 FT-IR spectrometer equipped with a liquid nitrogen cooled MCT (HgCdTe) detector using a sample cell with CaF_2 windows that were separated by 50 μm mylar spacers. Thin pellets of the dried MOF samples were incorporated between the two windows separated by the spacer. The spectrometer was purged continuously with dry air to remove water vapour. Typically, FT-IR spectra of 512 scans were taken with a resolution of 2 cm^{-1} and corresponding processing like background correction and base lining was performed using GRAMS software (Thermo Electron). The time between the assembly of cell and first spectrum collection was approximately as short as 2 min, which helped in minimizing the exposure of the MOFs to water vapour. For the conformational analysis of the CH_2 wagging modes of the alkoxy chains in the MOFs, the spectral region from 1400–1300 cm^{-1} was used. After baseline correction, the spectra were fitted using vibrational bands corresponding to *kinks* + *gtg*, *eg*, *dg* and CH_3 conformers using Gaussian and Lorentzian contributions applying GRAMS 8.0 software. During the fit analysis, the band positions were restricted to ± 2 cm^{-1} of their initial values given for each MOF. The integrated areas under the subbands were normalized with respect to the area of the standard reference band at 1320 cm^{-1} (C–O stretch). Details of the method and analysis can be found elsewhere.[15] Single crystal X-ray diffraction was performed on an Oxford Excalibur 2 diffractometer in a nitrogen cold stream (approx. 107 K) using Mo Kα radiation (λ = 0.71073 Å). The crystal structures were solved by direct methods using SHELXS-97 and refined against F^2 on all data by full-matrix least squares with SHELXL-97 (SHELX-97 program package, Sheldrick, Universität Göttingen, 1997).[16] The data of **2as** were treated with the "squeeze" routine in Platon[17] to account for the disordered 2-methoxyethoxy chains and solvent molecules. Powder X-ray diffraction (PXRD) patterns were recorded on a Bruker D8 Advance AXS diffractometer with Cu Kα radiation (λ = 1.54178 Å) and a Göbel mirror in $\theta - 2\theta$ geometry with a position-sensitive detector in a 2θ range from 5–50° at a scan speed of 1° min^{-1}. α-Al_2O_3 was employed as the external standard. The powder samples were filled into glass capillaries (diameter = 0.7 mm). Each capillary was sealed prior to the measurement. Thermogravimetric analyses (TGAs) were performed on a Seiko TG/DTA 6300S11 instrument (sample weight approximately 5–10 mg) at a heating rate of 5 °C min^{-1} in a temperature range from 30–600 °C. The measurement was performed at atmospheric pressure under flowing nitrogen (99.9999%; flow rate = 300 mL min^{-1}). N_2, CO_2 and CH_4 sorption measurements were performed on outgassed samples (130 °C for minimum 3 h *in vacuo*) using a Belsorb-Max from Bel-Japan with optimized protocols and gases of 99.9995% purity. N_2 measurements were performed at 77 K and 195 K. CO_2 and CH_4 measurements at 195 K.

Linker synthesis

The linkers were synthesized from three different starting compounds (Scheme 1), namely 2,3-dihydroxy-1,4-benzenedicarboxylic acid (S1), 2,5-dihydroxy-1,4-benzenedicarboxylic acid (S2), and 2,6-dihydroxy-1,4-benzenedicarboxylic acid (S3). S2 is commercially available, whereas S1 and S3 were synthesized in analogy to published procedures.[18,19] Accordingly, the starting compounds S1 to S3 were esterificated in MeOH with $BF_3 \cdot Et_2O$ as catalyst and water scavenger, to yield the dimethyl esters, dimethyl-2,3-dihydroxy-1,4-benzenedicarboxylate (S4), dimethyl-2,5-dihydroxy-1,4-benzenedicarboxylate (S5), and dimethyl-2,6-dihydroxy-1,4-benzenedicarboxylate (S6), which were dried in vacuum and characterized by ^1H and ^{13}C NMR spectroscopy. The particular linkers were synthesized *via* Williamson etherification of the compounds S4 to S6. In a typical reaction S4, S5, or S6 (4.40 mmol) and K_2CO_3 (20.0 mmol) were suspended in DMF (35 mL). RX (9.68 mmol, see Table 1 for the used halides) was added drop wise and the mixture was heated under stirring to 85 °C for 3 h. Afterwards the solvent was evaporated under reduced pressure at 60 °C and the residue was refluxed in H_2O (40 mL) with NaOH (10.0 mmol) for 4 h. After cooling to room temperature the solution was acidified with aqueous HCl (~15%) and the precipitate was collected by filtration, washed with water (20 mL) and dried *in vacuo* at 80 °C for 16 h (see Table 1 for the obtained yields). 2,3-Bis(2-methoxyethoxy)-1,4-benzenedicarboxylic acid, H_2(2,3-BME-bdc): ^1H NMR (250 MHz, DMSO): δ = 7.38 (s, 2H, Ar-H), 4.16–4.09 (m, 4H, OCH_2), 3.67–3.61 (m, 4H, OCH_2), 3.29 (s, 6H, OCH_3) ppm. ^{13}C NMR (63 MHz, DMSO): δ = 166.64, 151.34, 130.57, 124.36, 72.87, 70.96, 57.99 ppm. 2,6-Bis(2-methoxyethoxy)-1,4-benzenedicarboxylic acid, H_2(2,6-BME-bdc): ^1H NMR (250 MHz, DMSO): δ = 7.22 (s, 2H, Ar-H), 4.20–4.11 (m, 4H, OCH_2), 3.68–3.60 (m, 4H, OCH_2), 3.30 (s, 6H, OCH_3) ppm. ^{13}C NMR (63 MHz, DMSO): δ = 166.62, 165.90, 155.32, 132.73, 118.97, 106.16, 70.20, 68.30, 58.33. 2,5-Dimethoxy-1,4-benzenedicarboxylic acid, H_2(DM-bdc): ^1H NMR (250 MHz, DMSO): δ = 7.30 (s, 2H, Ar-H), 3.78 (s, 6H, OCH_3) ppm. ^{13}C NMR (63 MHz, DMSO): δ = 166.68, 151.07, 124.95, 114.41, 56.39 ppm. 2,5-Diethoxy-1,4-benzenedicarboxylic acid, H_2(DE-bdc): ^1H NMR (250 MHz, DMSO): δ = 7.26 (s, 2H, Ar-H), 4.04 (q, J = 6.9 Hz, 4H, OCH_2), 1.29 (t, J = 6.9 Hz, 6H, CH_3) ppm. ^{13}C NMR (63 MHz, DMSO): δ = 166.77, 150.31, 125.61, 115.73, 64.99, 14.64 ppm. 2,5-Dipropoxy-1,4-benzenedicarboxylic acid, H_2(DP-bdc): ^1H NMR (250 MHz, DMSO): δ = 7.26 (s, 2H, Ar-H), 3.94 (t, J = 6.3 Hz, 4H, OCH_2), 1.84–1.60 (m, 4H, CH_2), 0.97 (t, J = 7.4 Hz, 6H, CH_3) ppm. ^{13}C NMR (63 MHz, DMSO): δ = 166.78, 150.43, 125.46, 115.54, 89.84, 70.63, 22.08, 10.32 ppm. 2,5-Dibutoxy-1,4-benzenedicarboxylic acid, H_2(DB-bdc): ^1H NMR (250 MHz, DMSO): δ = 7.26 (s, 2H, Ar-H), 3.97 (t, J = 5.9 Hz, 4H, OCH_2), 1.76–1.57 (m, 4H, CH_2), 1.43 (dq, J = 14.1, 7.2 Hz, 4H, CH_2), 0.91 (t, J = 7.3 Hz, 6H, CH_3). ^{13}C NMR (63 MHz, DMSO): δ = 166.79, 150.41, 125.48, 115.50, 68.86, 30.77, 18.57, 13.63 ppm.

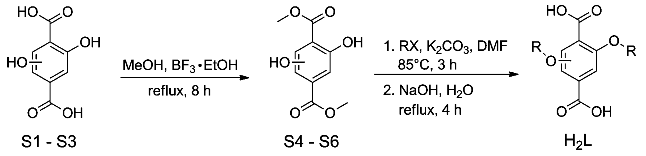

Scheme 1 Reaction sequence for the synthesis of the functionalized linkers H_2L. The utilized halides RX are listed in Table 1.

MOF synthesis

H_2L (L = 2,3-BME-bdc, 2,6-BME-bdc, DM-bdc, DE-bdc, DP-bdc, DB-bdc; 0.47 mmol), $Zn(NO_3)_2 \cdot 6H_2O$ (0.141 g, 0.47 mmol),

Table 1 Compilation of the halides (RX) used in the linker synthesis. The obtained yields are given in brackets

Linker (yield)	RX
2,3-BME-bdc (78%)	MeO–C_2H_4–Br
2,6-BME-bdc (65%)	MeO–C_2H_4–Br
DM-bdc (91%)	MeI
DE-bdc (85%)	EtBr
DP-bdc (89%)	PrBr
DB-bdc (84%)	BuBr

and 4,4′-bipyridine (0.074 g, 0.47 mmol) were dissolved in DMF (20 mL). EtOH (10 mL) was added and the reaction mixture was transferred into a screw jar, sealed and heated to 85 °C for 48 h to yield colourless crystals of **2as** and **4as** or colourless microcrystals of **3as**, **5as**, **6as**, and **7as**. After characterisation of the as synthesized compounds the mother liquor was decanted and the crystals were washed three times with DMF and then stirred for 3 days in chloroform (50 mL). The $CHCl_3$ was exchanged every 24 h against fresh solvent. Afterwards the pulverized material was collected by filtration and dried under reduced pressure ($\sim 10^{-3}$ mbar) for 24 h at 130 °C to achieve the dried MOFs (**2dry–7dry**), which were stored under inert gas atmosphere in a glovebox. Elemental analyses data (in weight%): $[Zn_2(2,3\text{-BME-bdc})_2(bipy)]_n$: C, 50.87 (50.07 theo); H, 4.78 (4.42 theo); N, 3.01 (3.07 theo); Zn, 14.02 (14.35 theo). $[Zn_2(2,6\text{-BME-bdc})_2(bipy)]_n$: C, 50.47 (50.07 theo); H, 5.02 (4.42 theo); N, 3.31 (3.07 theo); Zn, 13.98 (14.35 theo). $[Zn_2(DM\text{-bdc})_2(bipy)]_n$: C, 48.69 (49.00 theo); H, 3.56 (3.29 theo); N, 4.01 (3.81 theo); Zn, 17.83 (17.79 theo). $[Zn_2(DE\text{-bdc})_2(bipy)]_n$: C, 51.81 (51.60 theo); H, 4.43 (4.08 theo); N, 3.92 (3.54 theo); Zn, 16.14 (16.53 theo). $[Zn_2(DP\text{-bdc})_2(bipy)]_n$: C, 54.03 (53.85 theo); H, 5.00 (4.76 theo); N, 3.39 (3.31 theo); Zn, 15.19 (15.43 theo). $[Zn_2(DB\text{-bdc})_2(bipy)]_n$: C, 55.69 (55.83 theo); H, 5.60 (5.35 theo); N, 3.05 (3.10 theo); Zn, 14.22 (14.47 theo).

Results and discussion

Synthesis and structural characterisation

Analogous reactions of $Zn(NO_3)_2 \cdot 6H_2O$ with equimolar amounts of H_2L (L = 2,3-BME-bdc, 2,6-BME-bdc, DM-bdc, DE-bdc, DP-bdc, or DB-bdc) and bipy in DMF/EtOH solution (DMF = *N*,*N*-dimethylformamide) at 85 °C yield six novel MOFs of the composition $[Zn_2L_2(bipy)]_n$ (Schemes 2 and 3). The as synthesized compounds $[Zn_2(2,3\text{-BME-bdc})_2(bipy)]_n$ (**2as**) and $[Zn_2(DM\text{-bdc})_2(bipy)]_n$ (**4as**) form block like crystals, which were analysed *via* single crystal X-ray diffraction,† whereas the other four compounds (**3as**, **5as**, **6as**, and **7as**; L = 2,6-BME-bdc, DE-bdc, DP-bdc, or DB-bdc) give small intergrown microcrystals, only suitable for powder X-ray diffraction (PXRD).

After characterization by X-ray diffraction techniques, the as synthesized compounds were washed with fresh DMF and subsequently stirred in $CHCl_3$. Following, heating (130 °C) of the samples in dynamic vacuum ($\sim 10^{-3}$ mbar) gives the dried (activated) compounds $[Zn_2L_2(bipy)]_n$ (**2dry–7dry**), which were characterized by powder X-ray diffraction (PXRD), thermogravimetric analysis (TGA), as well as solid state ^{13}C MAS NMR and IR spectroscopy. In addition, liquid state ^1H and ^{13}C NMR spectra of digested MOF samples in $DCl/D_2O/[D_6]$DMSO were recorded, to prove the expected chemical composition. The dried MOFs were stored in a glovebox (Ar atmosphere) to avoid contact with water, because zinc-carboxylate based MOFs are in general quite sensitive to moisture.[13,20]

Surprisingly, **2as** does not crystallize in the expected honeycomb-like, trigonal structure. The single crystal structure reveals a tetragonal framework (space group *P*4/*mmm*) with a paddle-wheel-based pillared square-grid network (Fig. 2). Interestingly, the framework is non-interpenetrated due to the bulkiness of the 2-methoxyethoxy substituents, which do not leave enough void space to host a second framework. This has already been reported for other bulky linkers like 2,3,5,6-tetramethyl-1,4-benzenedicarboxylate.[10d] Because of the additional substituents, the carboxylate groups and the phenyl ring are no longer forced in a coplanar arrangement. Therefore, the phenyl ring can be in several positions. In the crystal structure of **2as** the 2,3-BME-bdc linkers connect the zinc paddlewheel in a bent and not a strictly linear fashion (Fig. 2b). Due to the bending the linker is disordered over two positions by the space group symmetry (see Fig. S2†). In addition the phenyl rings are disordered over two more positions. Due to this severe disorder the flexible 2-methoxyethoxy substituents could not be localized in the electron density map. However, ^{13}C MAS NMR of **2dry** as well as ^1H NMR and ^{13}C APT NMR of digested samples of **2dry** clearly prove the presence of the substituents (Fig. S13 and S19†).

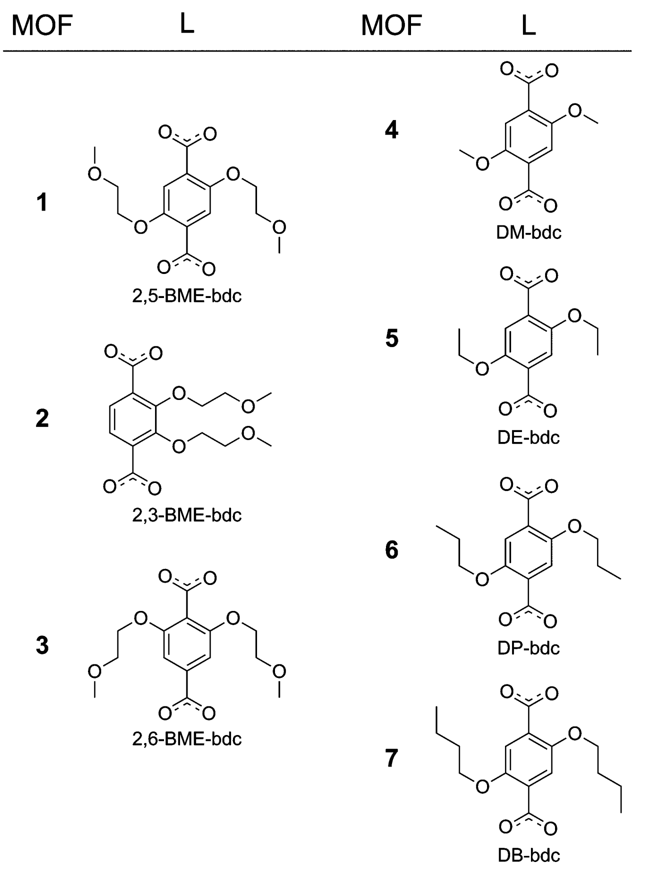

Scheme 2 Representation of the linkers L utilized in the $[Zn_2L_2(bipy)]_n$ MOFs **1–7**.

The phase purity of the bulk compound **2as** was analysed by PXRD (Fig. 3). The powder pattern features two rather weak reflections at $2\theta = 6.67°$ and $2\theta = 9.38°$, which can neither be indexed in the tetragonal unit cell derived from the single-crystal diffraction data nor in the trigonal unit cell of the honeycomb-like derivative **1as**. These reflections can be either dedicated to a minority phase, which arises from partial drying of the compound upon sample preparation (grinding of the crystals in air), or to the general presence of a second independent phase of unknown structure. Interestingly, the PXRD data of the activated, solvent-free compound **2dry** are mostly X-ray amorphous but show two weak reflections at $2\theta = 6.67°$ and $2\theta = 9.38°$ (Fig. S5†).

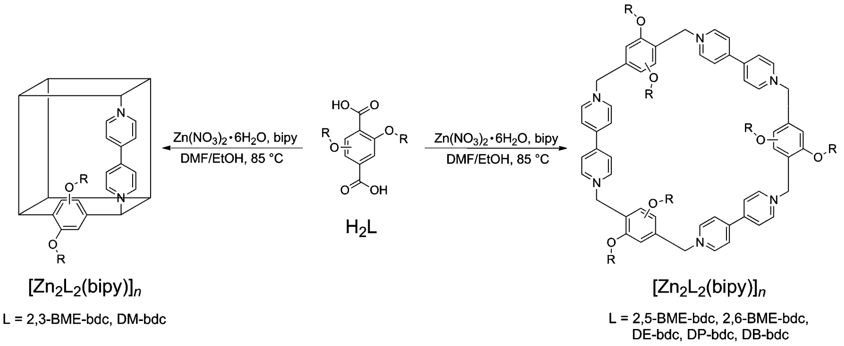

Scheme 3 Synthesis of $[Zn_2L_2(bipy)]_n$ MOFs. 2,3-BME-bdc triggers the formation of a non-interpenetrated pillared square-grid network (**2**) and DM-bdc prompts the formation of an interpenetrated pillared square-grid network (**4**). The other five linkers 2,5-BME-bdc, 2,6-BME-bdc, DE-bdc, DP-bdc, and DB-bdc generate $[Zn_2L_2(bipy)]_n$ MOFs featuring a honeycomb-like network topology (**1**, **3**, **5**, **6**, **7**).

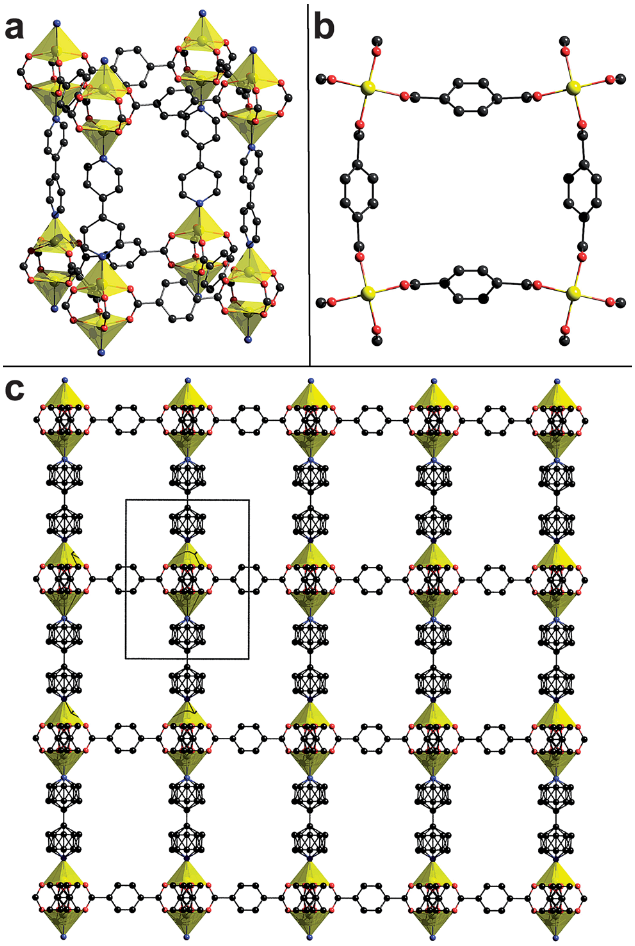

Fig. 2 Structure of $[Zn_2(2,3\text{-BME-bdc})_2(bipy)]_n$ (**2as**) as determined by single crystal X-ray diffraction: view of a cavity of the pillared square-grid network featuring a paddlewheel building unit (a), view of a fraction of the bent square-grid in the [001] direction (b), and packing diagram of the non-interpenetrated network along the [100] direction (c). Carbon, nitrogen, oxygen and zinc atoms are shown in dark grey, blue, red, and yellow, respectively. The coordination polyhedra around the zinc centres are shown in yellow. The severely disordered moieties of the linker 2,3-BME-bdc and bipy are not shown in (a) and (b). Flexible 2-methoxyethoxy groups, hydrogen atoms and guest molecules have not been refined due to the high disorder of the organic moieties and are not included in the structural model.

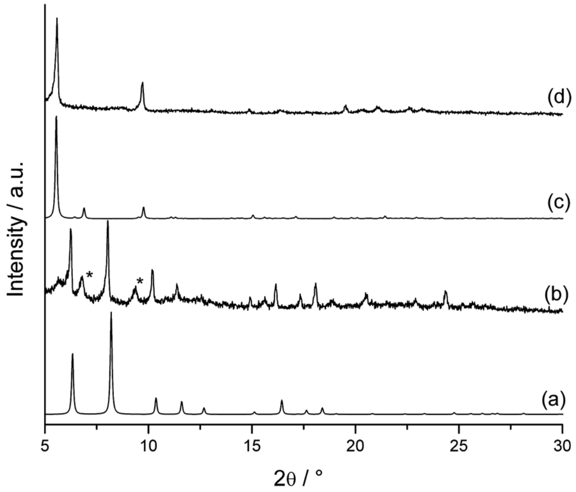

Fig. 3 Compilation of PXRD patterns: calculated diffraction pattern from the single crystal structure of **2as** (a), calculated pattern from the single crystal structure of **1as**[13] (c), measured patterns of **2as** (b), and **3as** (d). The reflections, which are marked with asterisks in (b), can be dedicated to a second minority phase of **2**, which is dedicated to partial drying of the material (see the ESI† for further details).

The changes in the powder patterns from **2as** to **2dry** suggest that the framework contracts and even decomposes when the solvent guests are evacuated. Note that we have already reported similar behaviours for other 2-methoxyethoxy functionalized MOFs.[14] The collapse of **2** upon activation seems to be irreversible, since renewed loading of **2dry** with DMF over the gas phase does not recover the initial crystalline structure of **2as**, but a different crystalline material (Fig. S5†). We suppose that the instability of **2** is reasoned in the large void volume of the non-interpenetrated network (58% void volume as analysed by Platon[17]) and the high framework flexibility, due to the attached 2-methoxyethoxy side chains.[14] However, a detailed analysis of the structural transitions occurring in **2** in dependence of the presence/absence of guest molecules turned out to be very complex and is beyond the scope of this work.

In comparison, compound **3as** features a honeycomb-like structure analogous to the parent framework **1as**, as determined by PXRD (Fig. 3). Indexation of the powder pattern in the trigonal space group $R\bar{3}c$ followed by a refinement of the unit cell parameters has proven phase purity (see Table S3†). Additionally, IR spectroscopy of **1dry**, **2dry**, and **3dry** manifests the analogy of **1** and **3**, whereas **2** gives a very different IR spectrum due to the different binding modes of the carboxylates in the honeycomb-like and in the pillared square-grid structure (Fig. 4). Therefore, the substitution pattern of the BME-bdc linkers has a major impact on the topology of the derived networks. MOFs **1**, **2**, and **3** are constructed from three different constitutional isomers of BME-bdc, which just differ in their substitution pattern.

To the best of our knowledge, this is the first example of topological MOF isomers, which present the same sum formula and have been prepared under exactly the same conditions, but form different network structures.

As already mentioned, the enhanced conformational freedom of the carboxylate groups of the functionalized linkers is essential to trigger the formation of the honeycomb-like network. The carboxylate groups of 2,3-BME-bdc and 2,5-BME-bdc should in principle possess similar conformational freedom. However, in 2,3-BME-bdc both substituents are located at the same side of the phenyl ring and would therefore point in the same channel of the honeycomb-like structure. This might lead to an overcrowding when 2,3-BME-bdc is utilized. Consequently, compound **2** forms the default pillared square-grid framework. Compound **3**, which utilizes 2,6-BME-bdc as linker, forms the honeycomb-like structure, although the substituents are both in *ortho*-position to one of the carboxylate groups. The substitution pattern suggests that only this carboxylate group possesses the enhanced conformational freedom, whereas the other carboxylate group located at position 4 is deemed to be coplanar to the phenyl ring. However, due to the lack of single crystal diffraction data a further discussion of the conformation of 2,6-BME-bdc in **3** cannot be provided.

We claim the trigonal honeycomb-like framework is thermodynamically more favoured, than the non-interpenetrated tetragonal structure, if BME-bdc-type linkers are used. The tetragonal isomer **2** has a much lower density ($\rho_{XRD} = 0.935$ g cm^{-3}) compared to the trigonal isomers **1** and **3** ($\rho_{XRD} = 1.249$ g cm^{-3}). Therefore, the void volume is much greater in the tetragonal topology. This higher void space may also be a reason for the collapse of **2** upon drying, while **1** and **3** retain their highly crystalline structure even after solvent exchange and drying at 130 °C *in vacuo* (Fig. S6†). Another big difference between both framework types is that the pillared layer structures exhibit intrinsic structural dynamics, due to the flexibility of the paddlewheel building unit,[10,11,14] whereas the honeycomb-like networks are structurally very rigid, because they are constructed from an infinite and inflexible one-dimensional building block. The higher stability of the honeycomb-like isomer is also evident from thermogravimetric analysis (TGA) data of the activated compounds, which show that the widely amorphous compound **2dry** starts to decompose at 200 °C, whereas the crystalline compounds **1dry** and **3dry** show no significant weight loss up to 300 °C (Fig. S11†).

Aside from the studies on the impact of the substitution pattern of BME-bdc on the framework structure of $[Zn_2L_2(bipy)]_n$ networks, we have analysed the impact of the substituent chain length for 2,5-substituted linkers. Therefore, the four differently functionalized linkers DM-bdc, DE-bdc, DP-bdc and DB-bdc (Scheme 1) were utilized together with zinc nitrate and bipy in the preparation of MOFs **4as**, **5as**, **6as**, and **7as**, respectively.

Interestingly, compound **4as** crystallizes in the monoclinic space group *C*2/*m*. Similar to **2as**, the network of **4as** is composed of two-dimensional square grids of $[Zn_2(DM\text{-}bdc)_2]_n$ units, which are pillared by bipy coligands (Fig. 5). Noteworthy, the aromatic rings of DM-bdc and bipy as well as the methoxy groups are disordered over two positions with 50% occupancy each (see ESI†). In analogy to $[Zn_2(bdc)_2(bipy)]_n$ the framework of **4** is doubly interpenetrated (Fig. 5 and S4†). PXRD studies of ground bulk samples of the as synthesized material **4as** harvested from the DMF/EtOH mother liquor, as well as the dried material **4dry**, show nearly identical patterns (Fig. S7†). Note that the

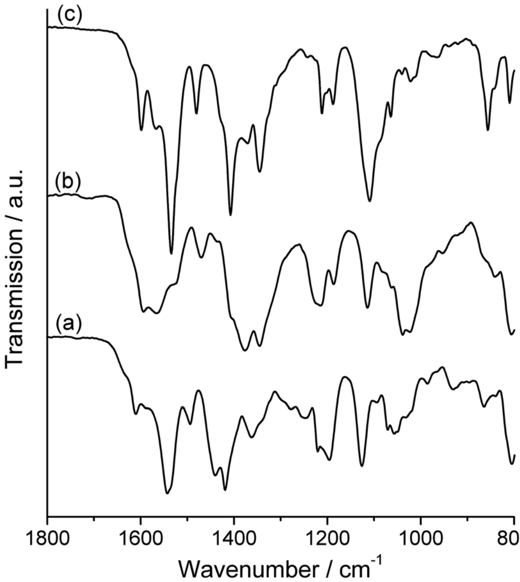

Fig. 4 ATR FT-IR spectroscopic data of dried **1dry** (a, taken from ref. 13), **2dry** (b), and **3dry** (c) displayed in the region from 800 to 1800 cm^{-1}.

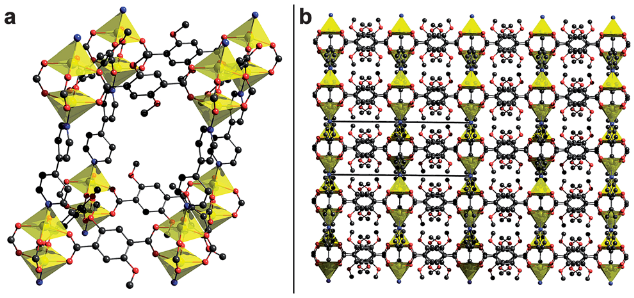

Fig. 5 Structure of $[Zn_2(DM\text{-}bdc)_2(bipy)]_n$ (**4as**) as determined by single crystal X-ray diffraction: view of a cavity of the pillared square-grid network featuring a paddlewheel building unit (a), packing diagram of the two-fold interpenetrated network along the [100] direction (b). Carbon, nitrogen, and oxygen atoms are shown in dark grey, blue and red, respectively. The coordination polyhedra around the zinc centres are shown in yellow. The second interpenetrating framework as well as disordered moieties of the linker DM-bdc and the pillar bipy are not shown in (a). Hydrogen atoms are omitted for the sake of clarity.

parent framework $[Zn_2(bdc)_2(bipy)]_n$ shows a structural transition (shrinkage of the unit cell volume) upon evaporation of guest molecules, which is leading to distinct changes of its PXRD pattern.[10b–d] However, **4** is structurally rigid and shows no framework flexibility. This can be attributed to a dense packing of the two interpenetrating nets of **4**, due to the higher steric demand of DM-bdc compared to the conventional bdc linker, leaving no accessible void volume. This was further validated by sorption experiments (N_2 at 77 K and CO_2 at 195 K), which show no gas uptake of **4dry** until saturation (data not shown). Therefore, **4as** and **4dry** feature the same chemical composition of $[Zn_2(\text{DM-bdc})_2(\text{bipy})]_n$.

Unfortunately, the compounds **5**, **6**, and **7** could only be obtained as small and intergrown crystals, which were not suitable for single crystal X-ray diffraction. However, indexation of the corresponding PXRD patterns and refinement of the unit cell parameters clearly show that these frameworks are isostructural and isoreticular to **1** and **3** (Fig. 6 and Table S3†). This is further validated by the similarity of the carboxylate stretching vibrations in the IR spectra of the activated compounds (Fig. 7, S26, and S28†).

Solid-state ^{13}C MAS NMR spectra of the honeycomb-like compounds **3dry**, **5dry**, **6dry**, and **7dry** feature two different signals for the carboxylate groups of the substituted linkers (Fig. S14 and S16–S18†). This can be dedicated to the presence of two distinct kinds of carboxylate groups in the honeycomb-like MOFs, namely carboxylates, which are bridging two zinc centres in a *syn–anti* fashion, and carboxylates, which are chelating just one zinc atom (Fig. 1). As expected ^{13}C MAS NMR spectra of **2dry** and **4dry** do only feature one signal for the carboxylate groups (Fig. S13 and S15†).

These results indicate that simple methoxy substituents do not have enough bulkiness to trigger the formation of the honeycomb-like topology, whereas the longer ethoxy, *n*-propoxy, and *n*-butoxy substituents yield structures isoreticular to **1**. If the linkers DE-bdc, DP-bdc, and DB-bdc would allow the formation of a pillared square-grid framework, these MOFs would be non-interpenetrated due to the bulkiness of the linkers. As seen for compound **2**, the non-interpenetrated frameworks are not so favourable because of the much higher void volume. Therefore, the bulky substituents trigger the formation of the honeycomb-like topology, which allows energetically favourable π interactions of the aromatic moieties as well as van der Waals interactions of the flexible substituents, and features a smaller void space per formula unit, compared to the non-interpenetrated pillared square-grid topology.

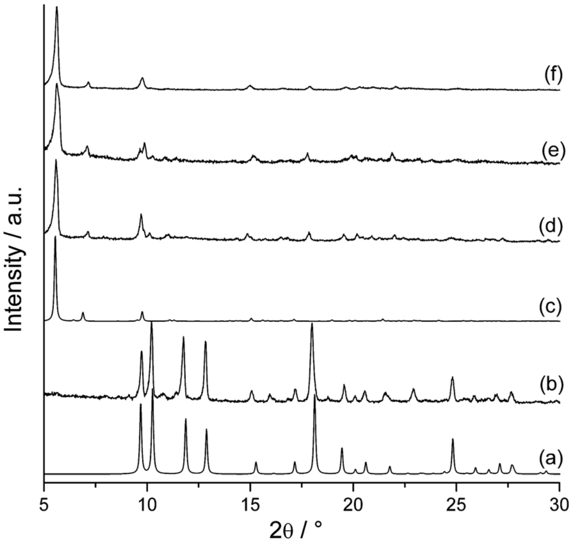

Fig. 6 Compilation of PXRD patterns: calculated diffraction pattern from the single crystal structure of **4as** (a), measured pattern of **4as** (b), calculated pattern from the single crystal structure of **1as**[13] (c), measured patterns of **5as** (d), **6as** (e), and **7as** (f).

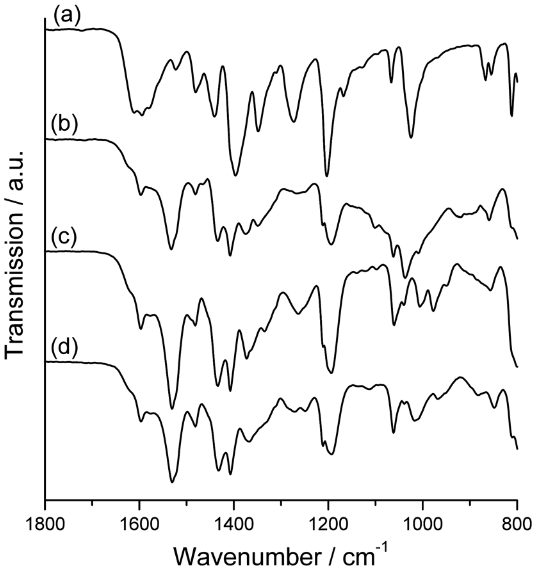

Fig. 7 ATR FT-IR spectroscopic data of **4dry** (a), **5dry** (b), **6dry** (c), and **7dry** (d) displayed in the region from 800–1800 cm^{-1}.

To get more information on the conformation of the flexible alkoxy chains in the honeycomb-like channel structures **5dry**, **6dry**, and **7dry** a detailed IR investigation has been conducted. Careful examination of the C–H stretching region between 3000 and 2800 cm^{-1} by band deconvolution suggests existence of several overlapping bands which can be assigned to CH_2 and CH_3 groups (Fig. S26†). The variation of the symmetric and asymmetric $\nu(CH_3)$ and $\nu(CH_2)$ bands with increasing chain length of the linker molecule suggests different conformations of the groups inside the pore. It is worth noting that these vibrations are observed in the dried and activated materials, and are expected to change markedly upon interaction with solvent and guest molecules. The spectral range from 1400–1300 cm^{-1} covers the conformation sensitive wagging modes of the CH_2 groups and the bands present there are due to various forms of *gauche* defects in the flexible alkoxy chains. The wagging modes of interest appear at 1363/1366 cm^{-1}, 1341/1342 cm^{-1}, 1349/1350 cm^{-1} and 1371/1378 cm^{-1} arising from the *gauche-trans-gauche* (*kinks* + *gtg*), *end gauche* (*eg*), *double gauche* (*dg*) and the methyl group "umbrella" deformation mode, respectively (see Fig. S27† for an illustration of the wagging modes). The *gtg* and *kinks* are taken together as a single class, since they cannot be spectroscopically distinguished from their CH_2 wagging modes. The band at 1319–1320 cm^{-1} arises from the C–O stretch of the linker and, due to its constant intensity, serves as the standard reference against which all the other wagging modes were ratioed to reveal the relative changes regarding the conformation of the flexible alkoxy chains in the different MOFs. Fig. 8 shows the conformation sensitive wagging region for **6dry** and **7dry**. The data of **5dry** were not used for the analysis here due to its short alkyl chain leading to a low signal to noise ratio, and the lack of possibility to form a multitude of different conformers.

For **6dry** the spectrum was decomposed by a curve fitting procedure and four wagging bands centered at 1341 cm^{-1} (*eg*), 1350 cm^{-1} (*dg*), 1363 cm^{-1} (*kinks* + *gtg*) and 1378 cm^{-1} (umbrella mode) were obtained. The band areas of these modes were then ratioed to the band area of the C–O stretch for calculating the relative populations of different conformers. A similar protocol was applied for **7dry**, here the bands are observed at 1342 cm^{-1} (*eg*), 1349 cm^{-1} (*dg*), 1366 cm^{-1} (*kinks* + *gtg*), and 1371 cm^{-1} (umbrella mode). Comparison of the normalized areas of the different subbands for these two MOFs leads to the following conclusions: **7dry** has on average (a) 3 times more *double gauche* conformers in its chains relative to **6dry**, (b) *ca.* 6 times more *kinks* + *gtg* conformers, and (c) the population of *end gauche* conformers is only about 20% higher for **7dry**. The contribution of the umbrella deformation mode is, as expected, essentially constant within the accuracy of the analysis. These results clearly state that the MOF with the longest flexible chain has a relatively high population of *kink* + *gtg* and *double gauche* conformers even in the solid state. The number of *end gauche* conformers does not vary markedly for these two MOFs as only two per chain are possible. It is interesting that even in confined geometry, **7dry** (longer alkoxy chain) exhibits a higher amount of disordered conformers than **6dry** (shorter alkoxy chain). This clearly suggests that the confined space is still favorable for the flexible substituents to exist in a multitude of conformations which would markedly increase without the confinement.

In future work we will concentrate on the IR spectroscopic analysis of such honeycomb-like MOFs, which are loaded with (solvent) guest molecules. In combination with the analysis of the wagging CH_2 mode region (1300–1400 cm^{-1}), the conformational properties of the alkoxy chain in solvent-filled pores will be accessible with residue specific resolution. Under these conditions, the population of disordered conformers is expected to increase. In addition, FT-IR spectroscopy will allow revealing also the conformation of the molecules embedded in the confined geometry of the MOFs.

Sorption properties of the honeycomb-like MOFs

The prototypic compound **1** shows beneficial sorption characteristics. **1dry** does not adsorb any N_2 at 77 K due to the gating of the pores with the polar and flexible 2-methoxyethoxy substituents. However, CO_2 can easily penetrate through the polar groups of **1dry** at 195 K. This leads to very high sorption selectivity for CO_2 compared to N_2 and CH_4 in this material ($S(CO_2/N_2) = 84 : 1$ and $S(CO_2/CH_4) = 9 : 1$ at 273 K estimated from the slopes of the isotherms in the Henry region).[13]

Here we have analysed the sorption properties of the isostructural compounds **5dry** and **7dry**. These MOFs feature only aliphatic substituents, without polar methoxy head groups, which are gating the pores. In comparison to **1dry**, N_2 sorption isotherms conducted at 77 K show that **5dry** and **7dry** adsorb very small, but significant amounts of nitrogen (Fig. 9) leading to rather low specific surface areas of 133 $m^2\ g^{-1}$ (**5dry**) and 35 $m^2\ g^{-1}$ (**7dry**) according to the BET model. The sorption kinetic for N_2 is very slow and a large hysteresis is visible on the desorption branches of both isotherms. The low adsorption capacities for N_2 again point out that the pores of the honeycomb-like frameworks

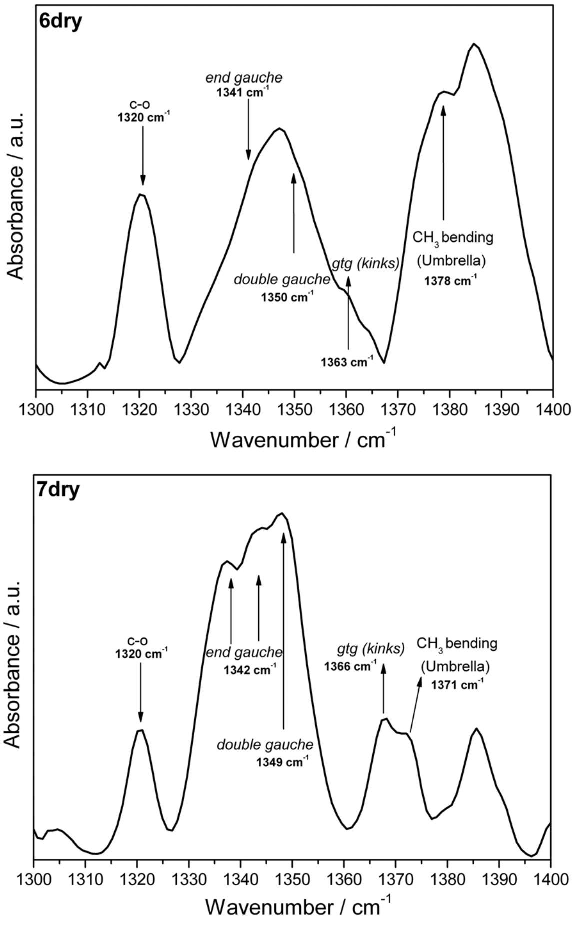

Fig. 8 FT-IR spectra of **6dry** and **7dry** for the wavenumber region between 1300 cm^{-1} and 1400 cm^{-1} showing the conformation sensitive CH_2 wagging bands.

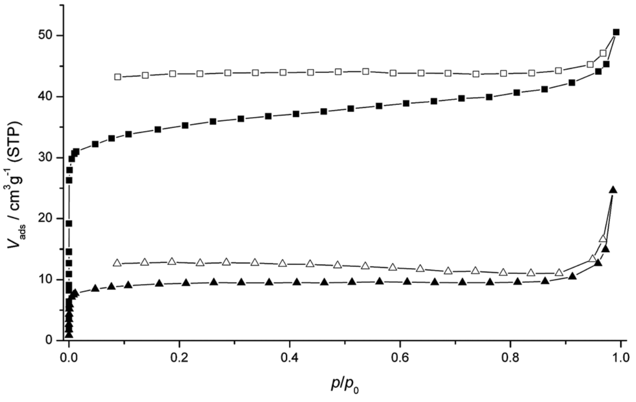

Fig. 9 Comparison of N_2 sorption isotherms for **5dry** (squares) and **7dry** (triangles) recorded at 77 K. The adsorption and desorption branches are shown by solid and open symbols, respectively.

are blocked by the flexible substituents at cryogenic temperatures.

A comparison of the N_2 isotherms recorded at 195 K yields no significant difference between the MOFs **1dry**, **5dry**, and **7dry** (Fig. 10). The CH_4 isotherms recorded at the same temperature show that **5dry** adsorbs a higher amount of CH_4, which is expected due to the lower density, higher void volume, and higher specific surface area of **5dry** compared to **1dry** and **7dry**. A similar trend can be seen in the CO_2 sorption isotherms. **5dry** can adsorb approx. 208 $cm^3\ g^{-1}$ (STP) CO_2 at saturation, whereas **1dry** and **7dry** adsorb 156 $cm^3\ g^{-1}$ (STP) and 128 $cm^3\ g^{-1}$ (STP), respectively. Noteworthy, **1dry** and **7dry** have nearly similar molecular weight ($M_{\mathbf{1dry}} = 911.51\ g\ mol^{-1}$; $M_{\mathbf{7dry}} = 903.61\ g\ mol^{-1}$), substituent chain length, density and accessible void volume. The fact that **1dry** adsorbs a higher amount of CO_2 than **7dry** can therefore be attributed to the polar 2-methoxyethoxy groups of **1dry**, which integrate a weakly Lewis basic pore environment that can interact stronger with the CO_2 molecules leading to a higher sorption selectivity for CO_2. A detailed examination of the CO_2 sorption isotherms (Fig. 10, bottom) indicates that **1dry** has the highest affinity for CO_2 at low pressures ($p < 7$ kPa) compared to **5dry** and **7dry** as evident by the steepest slope of the isotherm at low pressures. This can be attributed to the polar pore surface and the narrow confinement of **1dry**. However, as a matter of course at pressures greater than 7 kPa **5dry** adsorbs higher amounts of CO_2, because of its higher void volume. These results again reveal the beneficial impact of our concept to implement flexible and polar alkyl ether groups to tune the sorption selectivity of MOFs.[21]

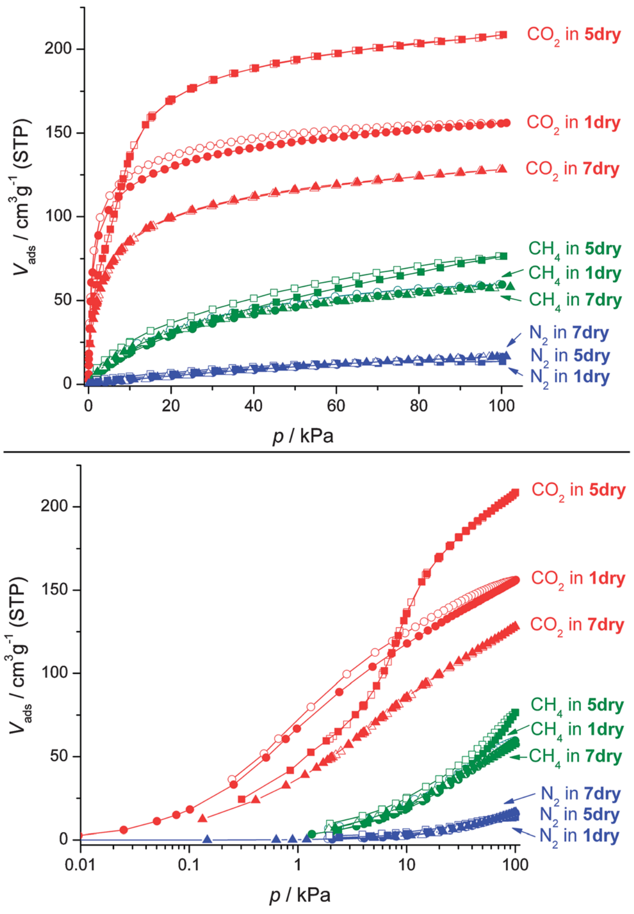

Fig. 10 Comparison of N_2 (blue), CH_4 (green), and CO_2 (red) sorption isotherms recorded at 195 K: isotherms for **1dry** (circles), **5dry** (squares), and **7dry** (triangles) plotted with a linear pressure axis (top) and a logarithmic pressure axis (bottom). The adsorption and desorption branches are shown with solid and open symbols, respectively. The sorption data of **1dry** were taken from ref. 13.

Conclusions

The targeted synthesis of specific framework architectures with attractive properties for an intended application is a major challenge for the development of new porous hybrid materials. With this systematic study we were able to sheet some light on the principles of the substitution dependent topological isomerism within the $[Zn_2L_2(bipy)]_n$ family of MOFs. Implementation of additional flexible side chains at the common linker 1,4-benzenedicarboxylate allows the construction of a novel honeycomb-like network family, which features interesting sorption properties. Remarkably, the substitution pattern of the bdc-type linker plays an important role for the derived framework topology. 2,3-Disubstitution of the bdc linker yields the formation of the well-known tetragonal pillared square-grid structure, whereas 2,5- and 2,6-disubstitution generates the novel honeycomb-like topology if 2-methoxyethoxy substituents are used.

Moreover, the chain length and bulkiness of the substituents have a great impact on the MOF topology. Small methoxy substituents do not have enough volume to force the framework in the honeycomb-like topology and give the interpenetrated pillared square-grid topology, whereas the more bulky ethoxy, *n*-propoxy, and *n*-butoxy substituents yield the honeycomb-like networks. These observations and effects are also suggested to be conceptually important to better understand solvent and templating effects in solvothermal MOF synthesis. Interestingly, our case study involves “solvent-like” molecules which are pinned at the linkers and therefore the weak forces between these groups and the more mobile solvent on the one side and interactions with the more rigid framework backbone on the other are likely to directly influence the crystallisation and phase selectivity as discussed above.

The sorption data of the honeycomb-like MOFs show that the use of methoxy head groups at the substituents increases the uptake and the sorption selectivity for CO_2 compared to simple non-polar aliphatic substituents. We hope that these results stimulate further research in the direction of substitution controlled MOF design and the development of novel framework topologies, which are inaccessible with conventional non-functionalized linkers.

Acknowledgements

S.H. gratefully thanks the Ruhr University Research School for a fellowship.

Notes and references

1 (*a*) J. R. Long and O. M. Yaghi, *Chem. Soc. Rev.*, 2009, **38**, pp. 1201–1508; (*b*) M. Eddaoudi, J. Kim, N. Rosi, D. Vodak, J. Wachter, M. O'Keeffe and O. M. Yaghi, *Science*, 2002, **295**, 469–472; (*c*)

S. Kitagawa, R. Kitaura and S. Noro, *Angew. Chem., Int. Ed.*, 2004, **43**, 2334–2375; (*d*) R. Robson, *Dalton Trans.*, 2008, 5113–5131; (*e*) U. Müller, M. Schubert, F. Teich, H. Puetter, K. Schierle-Arndt and J. Pastre, *J. Mater. Chem.*, 2006, **16**, 626; (*f*) G. Ferey, *Chem. Soc. Rev.*, 2008, **37**, 191–214.

2 (*a*) K. K. Tanabe and S. M. Cohen, *Chem. Soc. Rev.*, 2011, **40**, 498–519; (*b*) Z. Wang and S. M. Cohen, *Chem. Soc. Rev.*, 2009, **38**, 1315–1329; (*c*) H. Deng, C. J. Doonan, H. Furukawa, R. B. Ferreira, J. Towne, C. B. Knobler, B. Wang and O. M. Yaghi, *Science*, 2010, **327**, 846–850; (*d*) J. He, K.-K. Yee, Z. Xu, M. Zeller, A. D. Hunter, S. S.-Y. Chui and C.-M. Che, *Chem. Mater.*, 2011, **23**, 2940–2947; (*e*) K. S. Jeong, Y. B. Go, S. M. Shin, S. J. Lee, J. Kim, O. M. Yaghi and N. Jeong, *Chem. Sci.*, 2011, **2**, 877–882; (*f*) X. Zhang, F. X. Llabrés i Xamena and A. Corma, *J. Catal.*, 2009, **265**, 155–160; (*g*) A. M. Shultz, O. K. Farha, J. T. Hupp and S. T. Nguyen, *J. Am. Chem. Soc.*, 2009, **131**, 4204–4205; (*h*) T.-H. Park, K. Koh, A. G. Wong-Foy and A. J. Matzger, *Cryst. Growth Des.*, 2011, **11**, 2059–2063.

3 (*a*) M. Dinca and J. Long, *Angew. Chem., Int. Ed.*, 2008, **47**, 6766–6779; (*b*) R. Morris and P. Wheatley, *Angew. Chem., Int. Ed.*, 2008, **47**, 4966–4981; (*c*) D. M. D'Alessandro, B. Smit and J. R. Long, *Angew. Chem., Int. Ed.*, 2010, **49**, 6058–6082.

4 (*a*) J.-R. Li, R. J. Kuppler and H.-C. Zhou, *Chem. Soc. Rev.*, 2009, **38**, 1477–1504; (*b*) B. Chen, S. Xiang and G. Qian, *Acc. Chem. Res.*, 2010, **43**, 1115–1124.

5 (*a*) J. Y. Lee, O. K. Farha, J. Roberts, K. A. Scheidt, S. T. Nguyen and J. T. Hupp, *Chem. Soc. Rev.*, 2009, **38**, 1450–1459; (*b*) D. Farrusseng, S. Aguado and C. Pinel, *Angew. Chem., Int. Ed.*, 2009, **48**, 7502–7513; (*c*) M. Ranocchiari and J. A. van Bokhoven, *Phys. Chem. Chem. Phys.*, 2011, **13**, 6388–6396.

6 M. D. Allendorf, C. A. Bauer, R. K. Bhakta and R. J. T. Houk, *Chem. Soc. Rev.*, 2009, **38**, 1330–1352.

7 (*a*) M. D. Allendorf, R. J. T. Houk, L. Andruszkiewicz, A. A. Talin, J. Pikarsky, A. Choudhury, K. A. Gall and P. J. Hesketh, *J. Am. Chem. Soc.*, 2008, **130**, 14404–14405; (*b*) S. Achmann, G. Hagen, J. Kita, I. M. Malkowsky, C. Kiener and R. Moos, *Sensors*, 2009, **9**, 1574–1589; (*c*) G. Lu and J. T. Hupp, *J. Am. Chem. Soc.*, 2010, **132**, 7832–7833.

8 (*a*) Y. Takashima, S. Furukawa and S. Kitagawa, *CrystEngComm*, 2011, **13**, 3360–3363; (*b*) J. J. Zhang, L. Wojtas, R. W. Larsen, M. Eddaoudi and M. J. Zaworotko, *J. Am. Chem. Soc.*, 2009, **131**, 17040–17041; (*c*) S. R. Halper, L. Do, J. R. Stork and S. M. Cohen, *J. Am. Chem. Soc.*, 2006, **128**, 15255–15268; (*d*) S. Bauer, C. Serre, T. Devic, P. Horcajada, J. Marrot, G. Férey and N. Stock, *Inorg. Chem.*, 2008, **47**, 7568–7576.

9 (*a*) H. Furukawa, J. Kim, N. W. Ockwig, M. O'Keeffe and O. M. Yaghi, *J. Am. Chem. Soc.*, 2008, **130**, 11650–11661; (*b*) M. Eddaoudi, J. Kim, M. O'Keeffe and O. M. Yaghi, *J. Am. Chem. Soc.*, 2002, **123**, 376–377; (*c*) M. Eddaoudi, J. Kim, D. Vodak, A. Sudik, J. Wachter, M. O'Keeffe and O. M. Yaghi, *Proc. Natl. Acad. Sci. U. S. A.*, 2002, **99**, 4900–4904; (*d*) M. E. Braun, C. D. Steffek, J. Kim, P. G. Rasmussen and O. M. Yaghi, *Chem. Commun.*, 2001, 2532–2533.

10 See for example: (*a*) D. Dybtsev, H. Chun and K. Kim, *Angew. Chem., Int. Ed.*, 2004, **43**, 5033–5036; (*b*) B.-Q. Ma, K. L. Mulfort and J. T. Hupp, *Inorg. Chem.*, 2005, **44**, 4912–4914; (*c*) B. Chen, C. Liang, J. Yang, D. S. Contreras, Y. L. Clancy, E. B. Lobkovsky, O. M. Yaghi and S. Dai, *Angew. Chem., Int. Ed.*, 2006, **45**, 1390–1393; (*d*) H. Chun, D. N. Dybtsev, H. Kim and K. Kim, *Chem.–Eur. J.*, 2005, **11**, 3521–3529; (*e*) S. Horike, R. Matsuda, D. Tanaka, S. Matsubara, M. Mizuno, K. Endo and S. Kitagawa, *Angew. Chem., Int. Ed.*, 2006, **45**, 7226–7230; (*f*) B. Chen, S. Ma, E. J. Hurtado, E. B. Lobkovsky and H. C. Zhou, *Inorg. Chem.*, 2007, **46**, 8490–8492; (*g*) P. Maniam and N. Stock, *Inorg. Chem.*, 2011, **50**, 5085–5097; (*h*) K. Seki, *Chem. Commun.*, 2001, 1496–1497; (*i*) T. Takei, T. Ii, J. Kawashima, T. Ohmura, M. Ichikawa, M. Hosoe, Y. Shinya, I. Kanoya and W. Mori, *Chem. Lett.*, 2007, **36**, 1136–1137; (*j*) K. Uemura, Y. Yamasaki, Y. Komagawa, K. Tanaka and H. Kita, *Angew. Chem., Int. Ed.*, 2007, **46**, 6662–6665; (*k*) K. Uemura, Y. Yamasaki, F. Onishi, H. Kita and M. Ebihara, *Inorg. Chem.*, 2010, **49**, 10133–10143.

11 (*a*) S.-H. Cho, B. Ma, S. T. Nguyen, J. T. Hupp and T. E. Albrecht-Schmitt, *Chem. Commun.*, 2006, 2563–2565; (*b*) Y. Takashima, V. Martinez Martinez, S. Furukawa, M. Kondo, S. Shimomura, H. Uehara, M. Nakahama, K. Sugimoto and S. Kitagawa, *Nat. Commun.*, 2011, **2**, 168; (*c*) J. Seo, C. Bonneau, R. Matsuda, M. Takata and S. Kitagawa, *J. Am. Chem. Soc.*, 2011, **133**, 9005–9013.

12 (*a*) H. Chun and J. Moon, *Inorg. Chem.*, 2007, **46**, 4371–4373; (*b*) T. Frisic, D. G. Reid, I. Halasz, R. S. Stein, R. E. Dinnebier and M. L. Duer, *Angew. Chem., Int. Ed.*, 2010, **49**, 712–715; (*c*) M. Kondo, Y. Takashima, J. Seo, S. Kitagawa and S. Furukawa, *CrystEngComm*, 2010, **12**, 2350–2353.

13 S. Henke and R. A. Fischer, *J. Am. Chem. Soc.*, 2011, **133**, 2064–2067.

14 (*a*) S. Henke, R. Schmid, J.-D. Grunwaldt and R. A. Fischer, *Chem.–Eur. J.*, 2010, **16**, 14296–14306; (*b*) S. Henke, D. C. F. Wieland, M. Meilikhov, M. Paulus, C. Sternemann, K. Yusenko and R. A. Fischer, *CrystEngComm*, 2011, **13**, 6399–6404.

15 (*a*) O. Reis, R. Winter and T. W. Zerda, *Biochim. Biophys. Acta, Biomembr.*, 1996, **1279**, 5–16; (*b*) L. Senak, M. A. Davies and R. Mendelsohn, *J. Phys. Chem.*, 1991, **95**, 2565–2571.

16 G. M. Sheldrick, *Acta Crystallogr., Sect. A: Found. Crystallogr.*, 2008, **64**, 112–122.

17 A. L. Spek, *Acta Crystallogr., Sect. D: Biol. Crystallogr.*, 2009, **65**, 148–155.

18 (*a*) G. D. Lei, L. X. Li, Z. Y. Lu and M. G. Xie, *Chin. Chem. Lett.*, 2005, **16**, 1039–1042; (*b*) B.-C. Chen, M. S. Bednarz, J. E. Sundeen, Z. J. Zhang, T. J. Caulfield and G. S. Bisacchi, *Org. Prep. Proced. Int.*, 1999, **31**, 106–109; (*c*) S. P. Waters and M. C. Kozlowski, *Tetrahedron Lett.*, 2001, **42**, 3567–3570.

19 K. Brunner, N. Madersbacher and E. Goritschan, *Monatsh. Chem.*, 1928, **50**, 216–224.

20 (*a*) J. J. Low, A. I. Benin, P. Jakubczak, J. F. Abrahamian, S. A. Faheem and R. R. Willis, *J. Am. Chem. Soc.*, 2009, **131**, 15834–15842; (*b*) K. Schröck, F. Schröder, M. Heyden, R. A. Fischer and M. Havenith, *Phys. Chem. Chem. Phys.*, 2008, **10**, 4732–4739; (*c*) J. A. Greathouse and M. D. Allendorf, *J. Am. Chem. Soc.*, 2006, **128**, 10678–10679.

21 A. Bétard, H. Bux, S. Henke, D. Zacher, J. Caro and R. A. Fischer, *Microporous Mesoporous Mater.*, 2012, **150**, 76–82.